Applied Surface Science 364 (2016) 604–612

Contents lists available at ScienceDirect

Applied Surface Science

journal homepage: www.elsevier.com/locate/apsusc

Fabrication of novel magnetically separable BiOBr/$CoFe_2O_4$ microspheres and its application in the efficient removal of dye from aqueous phase by an environment-friendly and economical approach

R. Jiang[a,b,c], H.-Y. Zhu[a,b,c,*], J.-B. Li[b], F.-Q. Fu[a], J. Yao[a,c], S.-T. Jiang[c], G.-M. Zeng[d,**]

[a] Zhejiang Provincial Key Laboratory of Plant Evolutionary Ecology and Conservation, Taizhou University, Taizhou, Zhejiang 318000, PR China
[b] Environmental Engineering Program, University of Northern British Columbia, Prince George, British Columbia, Canada V2N 4Z9
[c] Department of Environmental Engineering, Taizhou University, Taizhou, Zhejiang 318000, PR China
[d] Key Laboratory of Environmental Biology and Pollution Control (Hunan University), Ministry of Education, Changsha 410082, PR China

ARTICLE INFO

Article history:
Received 19 September 2015
Received in revised form
23 December 2015
Accepted 26 December 2015
Available online 29 December 2015

Keywords:
Bismuth oxybromide
Cobalt ferrite
Photocatalysis
Decolorization
Congo red
Magnetic separation

ABSTRACT

Novel magnetically separable BiOBr/$CoFe_2O_4$ microspheres assembled from nanoparticles were successfully fabricated by a facile solvothermal method at 160 °C for 12 h. Then, BiOBr/$CoFe_2O_4$ microspheres were characterized via XRD, TEM, SEM, EDS and VSM. Congo red (CR) was selected as a pollutant model to evaluate the photocatalytic activities of BiOBr/$CoFe_2O_4$ microspheres. The value of coercivity (232 Oe) and the saturation magnetization (33.79 emu g^{-1}) were obtained, which indicated that BiOBr/$CoFe_2O_4$ microspheres can be separated and recovered easily from the treated solution. What is more, by calculation, the initial rate constants of BiOBr/$CoFe_2O_4$ microspheres is about 1.45 times higher than that of the pure BiOBr, which resulted from superior adsorption and transfer performance to organic contaminants in aqueous systems. Four consecutive regeneration cycles demonstrated that the BiOBr/$CoFe_2O_4$ microspheres had high photostability under simulated solar light irradiation. According to the radical trapping experiments, the h^+ radicals and $O_2^{\bullet -}$ radicals were the two main active species that drive the photocolorization of CR pollutant by BiOBr/$CoFe_2O_4$ microspheres under simulated solar light irradiation. This work suggests that the BiOBr/$CoFe_2O_4$ microspheres may be a promising photocatalyst for photodegrading organic pollutants and environmental remediation.

1. Introduction

The effective elimination of toxic organic pollutants discharged from industrial wastewater has become one of the most crucial aspects of contemporary pollution-control fields due to the harmful effects of those chemicals on the environment and aquatic living beings [1,2]. In the past few years, semiconductor photocatalysis driven by solar or visible light has attracted an extremely wide scientific and industrial attention for eliminating those organic pollutants in aqueous solution in an environmentally friendly manner [3–7].

Bismuth oxyhalides (i.e. BiOX) belong to the family of V–VI–VII semiconductor compounds, which are attracting considerable attention due to their excellent light photocatalytic activity and excellent electrical properties [8–12]. Among those of BiOX photocatalysts, bismuth oxybromide (BiOBr) has been recognized as one of the most promising photocatalysts owing to high photocatalytic activity, intrinsic lamellar structure and photostability [11,13–16]. However, as a semiconductor with a wide band gap (around 2.8 eV) [17], the absorption ability to visible light for the pure BiOBr is very limited for photodegrading toxic organic pollutants. Therefore, much efforts have been focused on combining BiOBr with other matching semiconductors, such as Ag_3PO_4 [15], Bi_2WO_6 [18], $BiPO_4$ [5,19], $ZnWO_4$ [17], C_3N_4 [20], CdS [4,21], PdS [22], and so on, to increase visible light absorption and efficient separation and transfer of photo-induced charge carriers. However, from the viewpoint of practical environment remediation, the effective and fast separation of fine photocatalysts from large volumes of treated solutions still remains a great challenge [23]. Fortunately, a convenient and viable solution to this problem is to combine semiconductor photocatalyst with some magnetic component which is easily separable by applying an external magnetic field [21,23–27].

* Corresponding author at: No. 1139, Municipal Government Avenue, Taizhou City, Zhejiang Province 318000, PR China.
** Corresponding author.
E-mail addresses: zhuhuayue@126.com (H.-Y. Zhu), zgming@hnu.cn (G.-M. Zeng).

http://dx.doi.org/10.1016/j.apsusc.2015.12.200
0169-4332/

Recently, spinel cobalt ferrite ($CoFe_2O_4$) nanoparticles have attracted great attention due to its obvious advantages of large saturation magnetization, good chemical stability, low cost, and environmental friendliness [28–38]. The large saturation magnetization of novel materials based on $CoFe_2O_4$ nanoparticles allows fast and effective separation of those materials from aqueous solution by a magnet [30,39,40]. In addition, enhanced visible-light-driven photoactivity has been observed over some composite semiconductors which combine $CoFe_2O_4$ with secondary material, such as TiO_2 [33], Ag/AgCl [26] and Pd (0) [41]. Furthermore, conventional porous structure of $CoFe_2O_4$ nanoparticles provides effective sites for removal of pollutants in aqueous solution [30,39,42,43]. Therefore, considering the advantages of both excellent photocatalytic performance of BiOBr and superior magnetic performance and high adsorption of $CoFe_2O_4$, it is feasible to construct stable and effective recoverable composite materials. However, to the authors' knowledge, there is rarely been exploited and reported the potentiality of magnetically separable BiOBr/$CoFe_2O_4$ microspheres for effective removal of dye pollutant from aqueous environments.

In this work, novel magnetically separable BiOBr/$CoFe_2O_4$ microspheres with high adsorption-photocatalysis and excel magnetic performance were synthesized by a facile solvothermal method at 160 °C for 12 h. Then, BiOBr/$CoFe_2O_4$ microspheres were characterized via X-ray diffraction (XRD), transmission electron microscopy (TEM), scanning electron microscopy (SEM), energy dispersive spectroscopy (EDS) and vibrating sample magnetometry (VSM). The excellent photocatalytic activity of the as-prepared BiOBr/$CoFe_2O_4$ microspheres was evaluated by photocatalytic decolorization of dye Congo red (CR) solution under simulated solar light irradiation. The photocatalytic stability of BiOBr/$CoFe_2O_4$ microspheres was evaluated. In addition, the possible mechanism of enhanced photocatalytic activity was also discussed. This study provides a promising candidate for efficient removal of dye solution by an environment-friendly and economical approach.

2. Experimental

2.1. Chemicals

$Co(NO_3)_2{\cdot}6H_2O$, $Fe(NO_3)_3{\cdot}9H_2O$, $Bi(NO_3)_3{\cdot}5H_2O$, KBr and ethylene glycol were purchased from Shanghai Chemical Reagents Research Institute (Shanghai, China). Congo red (abbreviated as CR) as a model dye was purchased from Yongjia Fine Chemical Factory (Wenzhou, China). All chemicals were analytical grade and used without further purification. Double distilled water was used in the preparation of photocatalysts and subsequent photocatalytic experiments.

2.2. Preparation of $CoFe_2O_4$ nanoparticles

$CoFe_2O_4$ nanoparticles were synthesized using a revised solvothermal method [28,36]. The stoichiometric amount of cobalt nitrate ($Co(NO_3)_2{\cdot}6H_2O$) and iron nitrate ($Fe(NO_3)_3{\cdot}9H_2O$) was dissolved in distilled water (25 mL) to obtain a mixed solution under vigorous stirring for 2 h using a magnetic stirrer at room temperature. The molar ratio of Co^{2+} to Fe^{3+} was 0.5. The pH of the solution was adjusted to 12 by adding 4 M NaOH solution. Then, the mixture was further transferred into a 100 mL Teflon-lined autoclave and subsequently heated at 180 °C for 12 h. After the reaction was completed, the solid sample was separated from the system by applying an external magnetic field and was washed several times with distilled water with the aid of ultrasonic techniques. The resulting powder was finally dried at 60 °C for 12 h till constant weight.

2.3. Preparation of BiOBr/$CoFe_2O_4$ microspheres

BiOBr/$CoFe_2O_4$ microspheres were synthesized by a facile solvothermal method. 3 mmol of $Bi(NO_3)_3{\cdot}5H_2O$ and 3 mmol of KBr were initially dissolved in 60 mL ethylene glycol and sonicated for 30 min at room temperature. Then, 0.3920 g of as-prepared magnetic $CoFe_2O_4$ nanoparticles was dispersed into the resulting solution. After vigorously stirring for another 40 min, the resulting suspension was transferred into a 100 mL Teflon-lined stainless steel autoclave and heated to 160 °C for 12 h, and then the autoclave was cooled down naturally. After the reaction was completed, the sample was separated from the system by applying an external magnetic field and was washed with ethanol and distilled water several times, respectively, with the aid of ultrasonic techniques. The product was finally dried at 60 °C for 12 h till constant weight. The samples with different BiOBr/$CoFe_2O_4$ weight ratio of 9:1, 7:3 and 5:5 were named as BC9, BC7 and BC5.

For comparison, pure BiOBr microspheres were prepared by refereeing to a previous study [16]. First, 3 mmol of $Bi(NO_3)_3{\cdot}5H_2O$ and 3 mmol of KBr were dissolved in 60 mL ethylene glycol under vigorous stirring to obtain a transparent solution. Then, the resulting solution was transferred into a 100 mL Teflon-lined stainless steel autoclave and heated to 160 °C for 12 h. After the reaction was completed, the sample was separated by centrifugation and washed with absolute ethanol and distilled water, respectively. The product was finally dried at 60 °C for 12 h till constant weight.

2.4. Characterization of BiOBr/$CoFe_2O_4$ microspheres

X-ray powder diffraction (XRD) analysis was performed on a Bruker AXS D8-advance X-ray diffractometer with Cu Kα radiation in the 2θ range of 10°–70°. UV–Vis diffuse reflectance spectra (UV–Vis DRS) were carried out by an UV-3100 UV–vis spectrophotometer (Hitachi Corporation, Japan). The morphology and microstructure of the synthesized samples were characterized by a scanning electron microscopy (SEM, Hitachi S4800 equipped with an EDS). Transmission electron microscopy (TEM) and high resolution Transmission electron microscopy (HRTEM) were performed on an FEI Tecnai G20 with field- emission gun operating at 200 kV. The specific surface area and pore diameter measurements were carried out using an MPMS-XL-7 surface area and porosity analyzer (Quantum Design, America). Magnetization measurements were carried out on an MPM5-XL-5 superconducting quantum interference device (SQUID) magnetometer in an external field up to 15 kOe at room temperature (20 °C).

2.5. Photocatalytic experiments

The photocatalytic experiments were performed by the decolorization of CR solution under simulated solar light irradiation in a photochemical reactor (Nanjing Xujiang Electromechanical Factory, Nanjing, China) at constant room temperature (20 °C) (Fig. 1). A 300 W xenon lamp was used as a simulated solar light source, which was positioned in the cylindrical quartz trap and surrounded by cooling water. In a typical experiment, 30 mg of the photocatalyst was dispersed into a 30 mL CR solution (15 mg L^{-1}). Then, the dispersion was exposed to simulated solar light irradiation. During photocatalytic reaction, the aqueous suspension containing CR and photocatalyst was continuously stirred and bubbled so that the concentration of dissolved oxygen in reaction system was kept constant. At given time intervals, 5 mL of dispersion was drawn and BiOBr/$CoFe_2O_4$ microspheres were separated immediately by a magnet. Residual CR concentration in supernatant was analyzed at λ_{max} = 496.0 nm using a TU 1810 UV–visible spectrophotometer (Beijing Purkinje General Instrument Co., Ltd, China).

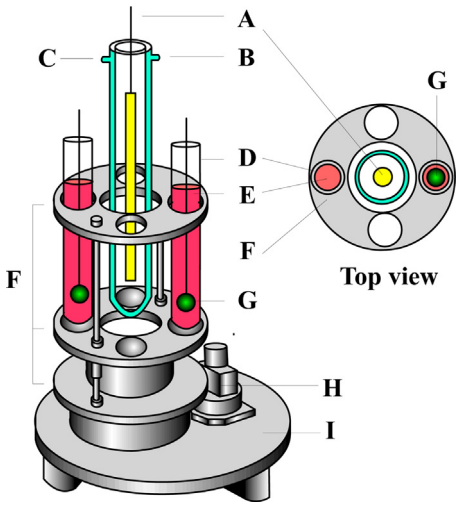

Fig. 1. Reactor used in the photocatalytic experiments. A. xenon lamp; B. cooling water inlet; C. cooling water outlet; D. quartz reactor; E. dye solution; F. rotating disks; G. aeration head; H. electric machinery; and I. pedestal.

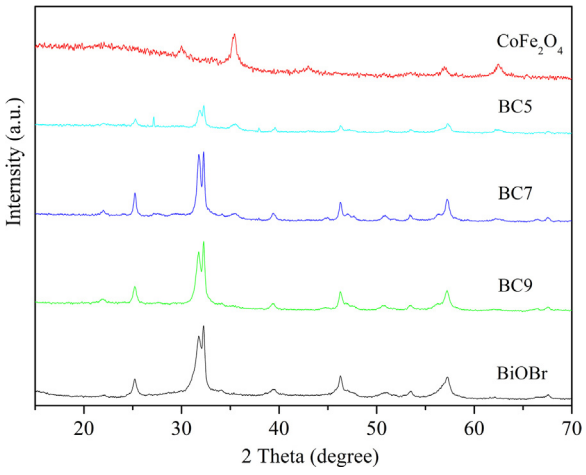

Fig. 2. XRD patterns of BiOBr, $CoFe_2O_4$ and BiOBr/$CoFe_2O_4$ microspheres.

Decolorization efficiency (η) of CR solution by BiOBr/$CoFe_2O_4$ microspheres at time t was calculated by Eq. (1).

$$\eta(\%) = \frac{(C_0 - C_t)}{C_0} \times 100 \quad (1)$$

where C_0 and C_t (mg L^{-1}) are the initial CR concentration and the CR concentrations at any time t (min), respectively.

3. Results and discussion

3.1. Characterization of as-synthesized samples

3.1.1. XRD

The phase structure of the as-prepared BiOBr, $CoFe_2O_4$ and BiOBr/$CoFe_2O_4$ microspheres were investigated by XRD analysis (Fig. 2). It can be easily found that the diffraction peaks on $CoFe_2O_4$ at $2\theta = 30.03^\circ$, 35.48°, 43.03°, 56.94° and 62.49° were completely matched the reflections of (2 2 0), (3 1 1), (4 0 0), (5 1 1) and (4 4 0), respectively, indexed to the cubic spinel structure of $CoFe_2O_4$ (JCPDS 22-1086) [29,40,44]. The mean size of the $CoFe_2O_4$ crystallites calculated from the diffraction patterns was about 21 nm. The pure BiOBr sample showed a tetragonal crystal phase with the detected reflections at 22.13° (0 0 2), 25.21° (1 0 1), 31.69° (1 0 2), 32.27° (1 1 0), 39.35° (1 1 2), 46.29° (2 0 0), 50.7° (1 0 4) and 57.25° (2 1 2) (JCPDS 78-0348) [16,19,44,45]. No crystalline $CoFe_2O_4$ can be detected from the BC9 with low $CoFe_2O_4$ concentrations, whereas two main peaks of $CoFe_2O_4$ at $2\theta = 35.28^\circ$ (3 1 1) and 62.49° (4 4 0) were found from XRD patterns of BC7 and BC5, indicating the coexistence of $CoFe_2O_4$ and BiOBr in BC7 and BC5. In addition, the peak of BiOBr decreased gradually in intensity with the increase of $CoFe_2O_4$ content. The XRD diffraction of BC5 shows small impurities at $2\theta = 27.27^\circ$, indicating that there is a small amount of impurity coexisting with diffraction of $CoFe_2O_4$ and BiOBr.

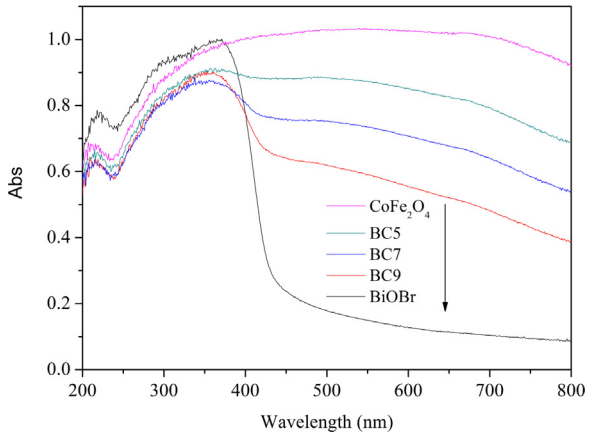

Fig. 3. UV–vis DRS of BiOBr, $CoFe_2O_4$ and BiOBr/$CoFe_2O_4$ microspheres.

3.1.2. UV–Vis DRS

It is well known that the photoinduced charge-transfer property and enhanced light photocatalytic activity of semiconductors in the photocatalytic reaction are closely related to their optical properties [46]. Thus, the optical absorbance of as-prepared photocatalyst was measured by UV–visible diffuse reflectance spectra (DRS). The corresponding results are shown in Fig. 3. Obviously, pure BiOBr only has weak absorption in visible light region with an absorption edge around 442 nm and has a band gap of 2.81 eV, which is slightly larger than the values reported in previous literatures [11,13]. However, the absorption intensity of $CoFe_2O_4$ is very strong in both visible light and UV region from 200 nm to 800 nm, which results from the black appearance of pure $CoFe_2O_4$ material [26]. With the increase of $CoFe_2O_4$ content, the absorption in visible light region increased obviously and strengthened gradually due to the strong visible light response of $CoFe_2O_4$. The result is in agreement with the color change of the samples from yellow to black. In previous study, an obvious red-shift was also observed when BiOBr microsphere formed a heterojunction with other black materials [24]. The excel photocatalytic activity of the BiOBr/$CoFe_2O_4$ could be expected under simulated solar light irradiation since BiOBr/$CoFe_2O_4$ microspheres exhibit an enhanced absorption in the whole visible light region compared with the pure BiOBr.

3.1.3. SEM and TEM

The morphology of pure BiOBr, $CoFe_2O_4$ and BiOBr/$CoFe_2O_4$ microsphere were characterized by SEM (Fig. 4) and TEM (Fig. 5). It can be seen from Fig. 4a, pure BiOBr has a waxberry-like microspheres, and the diameter is in the range of 2–5 μm [16]. As can be seen from the high-magnification SEM image (Fig. 4b), the individual waxberry-like BiOBr microsphere was self-assembled by numerous interleaving nanocrystalline sheets with a thickness from 20 nm to 30 nm [16]. The pure cobalt ferrites were nanocrystalline and their shape is spherical in the size range of 30–25 nm (Fig. 4c) [36]. The BiOBr/$CoFe_2O_4$ composite exhibits microsphere shapes with an average diameter of 5 μm (Fig. 4d). The enlarged images in Fig. 4 e clearly showed that the surface of the

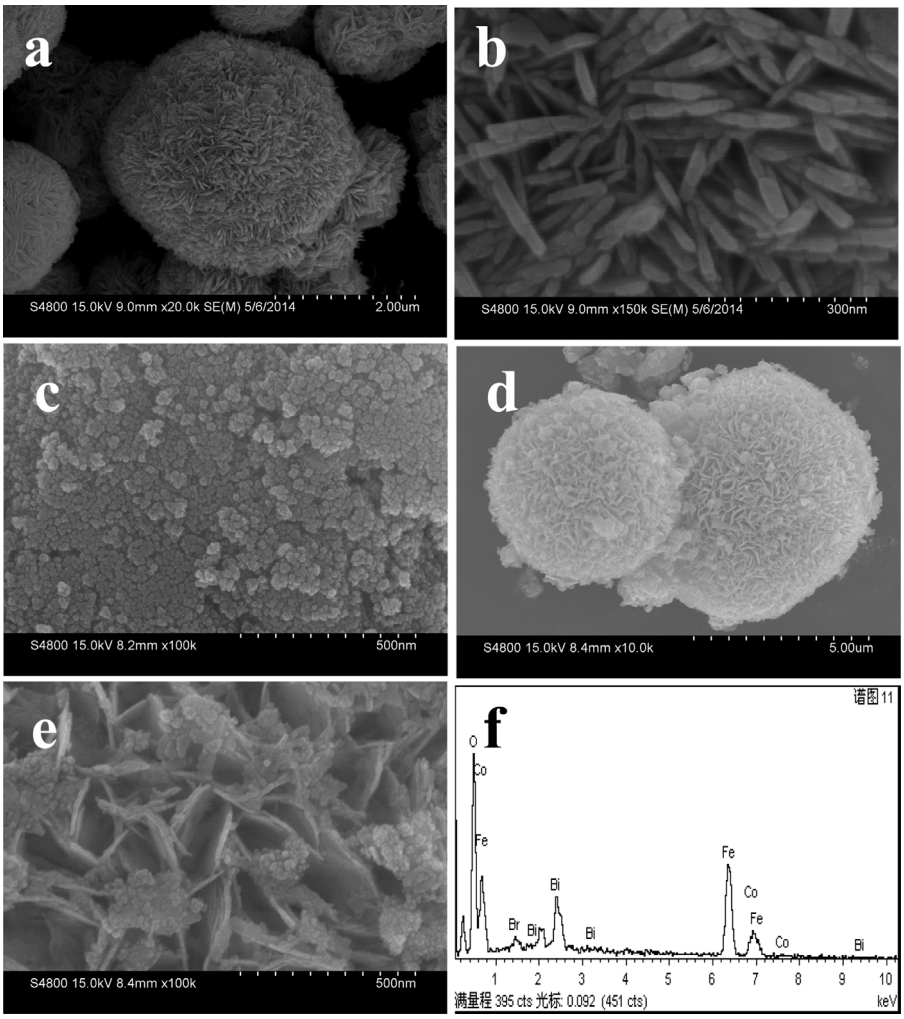

Fig. 4. SEM images of the pure BiOBr (a and b), the pure $CoFe_2O_4$ (c), the hierarchical heterostructured BiOBr/$CoFe_2O_4$ microspheres (d and e) and the EDS of BiOBr/$CoFe_2O_4$ microspheres.

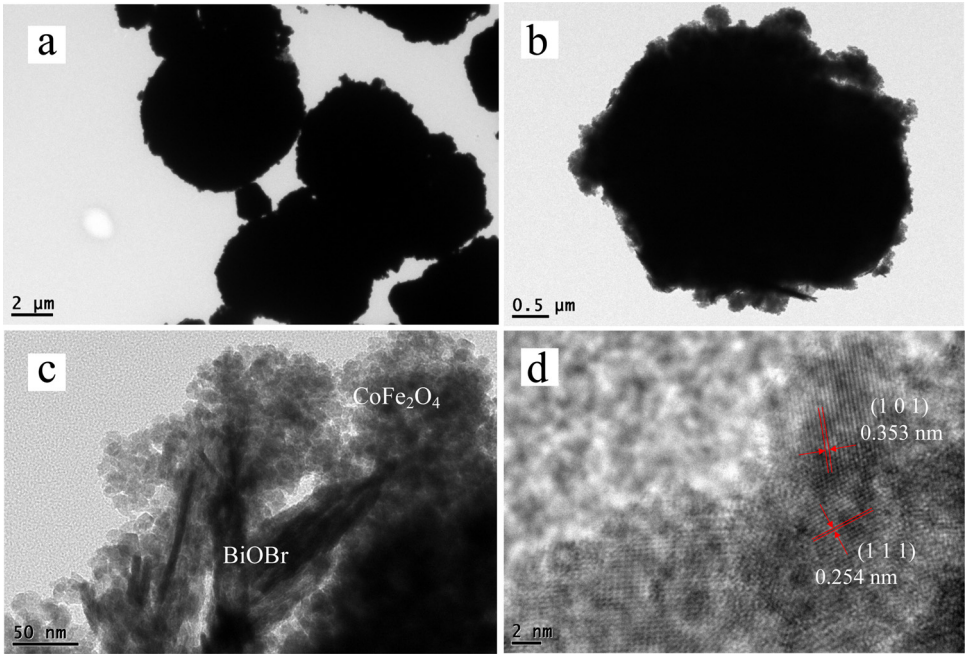

Fig. 5. TEM images of BiOBr/$CoFe_2O_4$ microspheres.

waxberry-like BiOBr microspheres were stuck with some tiny nanoparticles, indicating that $CoFe_2O_4$ nanoparticles have been interspersed on BiOBr microsphere. The existence of $CoFe_2O_4$ nanoparticles could facilitate the separation of the photoinduced electron–hole pairs effectively [34] and convenient recovery from treated solution [30,39]. Those rough surfaces of the BiOBr/$CoFe_2O_4$ microsphere enlarge their surface areas and provide more sizes for adsorption of pollutant molecules [42,47]. The EDS analysis of the BiOBr/$CoFe_2O_4$ microspheres (Fig. 4f) suggests that the sample contains only the elements Br, O, Bi, Fe and Co. Both results of SEM and EDS indicate that the BiOBr/$CoFe_2O_4$ microspheres can be obtained under the present synthetic conditions.

The low-magnified and high-magnified TEM images of BiOBr/$CoFe_2O_4$ microspheres are shown in Fig. 5. As revealed in Fig. 5a and b, the as-prepared BiOBr/$CoFe_2O_4$ microspheres have a round shape. The high resolution TEM image clearly shows that the BiOBr/$CoFe_2O_4$ microspheres composed of many small nanoparticles (about 10.3 nm) and nanoplates (Fig. 5c). There are the fringes with the lattice spacing of 0.254 nm and 0.353 nm, which could be indexed to the (3 1 1) plane of $CoFe_2O_4$ and (1 0 1) plane of BiOBr, respectively (Fig. 5d) [16,48].

3.1.4. Adsorption–desorption isotherm, pore structure, and specific surface areas

The enhanced photocatalytic performance of photocatalysts could be mainly attributed to excellent physicochemical properties including higher surface areas [49]. The specific surface area and porosity of samples were investigated by measuring the nitrogen adsorption isotherms, as shown in Fig. 6. N_2 adsorption and desorption processes of both BiOBr and BiOBr/$CoFe_2O_4$ microspheres exhibit similar type IV curves, which is typically characteristic of mesoporous materials [50]. Such mesoporous structure is very beneficial for the diffusive transport of photoinduced carriers to oxidized species. The BET surface areas of BiOBr and BiOBr/$CoFe_2O_4$ microspheres calculated from the isotherms are 8.33 ± 0.11 and $74.84 \pm 1.16\ m^2\ g^{-1}$, respectively. Obviously, BiOBr/$CoFe_2O_4$ microspheres have a larger surface area than BiOBr microspheres since $CoFe_2O_4$ nanoparticles have a smaller particle size and a relative larger surface area ($116.4\ m^2\ g^{-1}$) [35]. Compared with other reported photocatalysts based on BiOBr, such as BiOBr/Fe_2O_3 [24], BiOBr/Fe_3O_4 [24], BiOBr/Co-Ni-NO_3 LDHs [49], BiOBr/fly-ash [11], the surface area of obtained BiOBr/$CoFe_2O_4$ microspheres is relatively large, which resulted in providing more reactive centers, absorbing more pollutant molecules and promoting the efficiency of electron–hole separation [51]. In addition, as shown in the inset of Fig. 6a and b, BiOBr/$CoFe_2O_4$ microspheres display wider pore size distributions than BiOBr. As a result, it is very reasonable to expect that BiOBr/$CoFe_2O_4$ microspheres have potential for the efficient removal of pollutants since it can provide more active species and more organic reactants on its surface.

3.1.5. VSM

Fig. 7a presents plots of magnetization versus the applied external magnetic field at room temperature for $CoFe_2O_4$ and BiOBr/$CoFe_2O_4$ microspheres. The VSM curves of the $CoFe_2O_4$ show that saturation magnetization was $54.83\ emu\ g^{-1}$ at 10,000 Oe (Fig. 7a), which is higher than the values of $CoFe_2O_4$ prepared by different reported methods [38,52]. Size and shape anisotropy here play critical roles in determining magnetic properties [37]. With the assembly of $CoFe_2O_4$ powders on the surface of BiOBr microspheres, the saturation magnetization of BiOBr/$CoFe_2O_4$ microspheres decreases to $33.79\ emu\ g^{-1}$ at 10,000 Oe. Such a decrease could be resulted from the presence of nonmagnetic component [24]. However, the saturation magnetization of BiOBr/$CoFe_2O_4$ microspheres is still higher than those reported values of other magnetic photocatalysts [24,53]. The coercivity

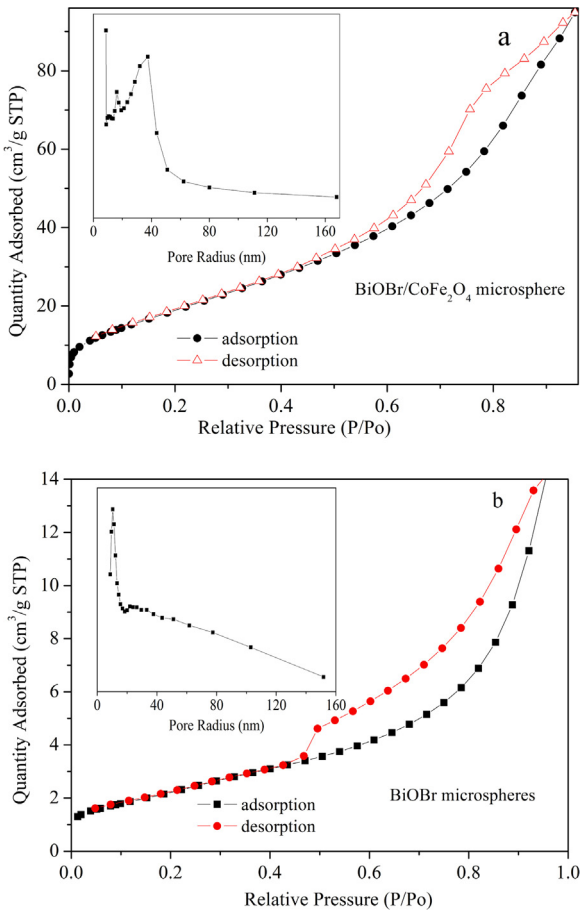

Fig. 6. Nitrogen adsorption and desorption isotherms and corresponding pore size distributions (inset) of (a) hierarchical BiOBr/$CoFe_2O_4$ microspheres and (b) hierarchical BiOBr microspheres.

value decreases from 537 to 232 Oe with the introduction of BiOBr (Fig. 7a inset). The result shows that BiOBr/$CoFe_2O_4$ microspheres display expectant magnetic performance and can be separated and recovered easily from the treated solutions after liquid-phase photocatalytic reaction (Fig. 7b), which could facilitate the practical running of an industrial wastewater treatment.

3.2. Photocatalytic activity of as-synthesized samples

To demonstrate the potential application of the BiOBr/$CoFe_2O_4$ microspheres in the photocatalytic degradation of dye pollutant, the photocatalytic activities of BiOBr/$CoFe_2O_4$ microspheres with different $CoFe_2O_4$ loadings were evaluated firstly. From the results displayed in Fig. 8, BiOBr/$CoFe_2O_4$ microspheres showed obviously higher photocatalytic activity than pure BiOBr microspheres. The photocatalytic activity of BiOBr/$CoFe_2O_4$ microspheres is closely related to $CoFe_2O_4$ loading. After 60 min visible light irradiation, 62.27%, 71.17%, 85.61% and 90.78% of CR solution have been decolorized by the as-synthesized samples BiOBr, BC9, BC7 and BC5, respectively. The results showed that the introduction of $CoFe_2O_4$ has enhanced photocatalytic performance [54]. The sharp decrease in absorption peak intensity and the fading observed for the CR solution within 60 min also indicate that BiOBr/$CoFe_2O_4$ exhibits excellent photocatalytic activity on degradation of the CR solution. Photocatalytic decolorization of dye solution by photocatalyst follows the Langmuir–Hinshelwood kinetic model when the reactant concentration is low [3,55]. By calculation, the initial rate constant ($0.1594\ min^{-1}$) of BiOBr/$CoFe_2O_4$ microspheres is about 2.45 times

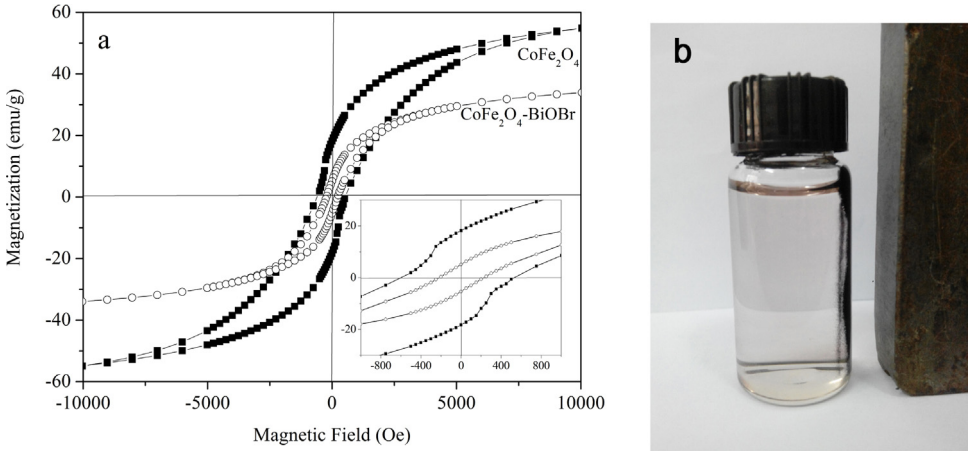

Fig. 7. (a) Magnetization curves of $CoFe_2O_4$, the $BiOBr/CoFe_2O_4$ microspheres measured at room temperature (the inset is the corresponding magnetization of the low field (−2000 to 2000 Oe)) and (b) the separation of $BiOBr/CoFe_2O_4$ microspheres by a magnet.

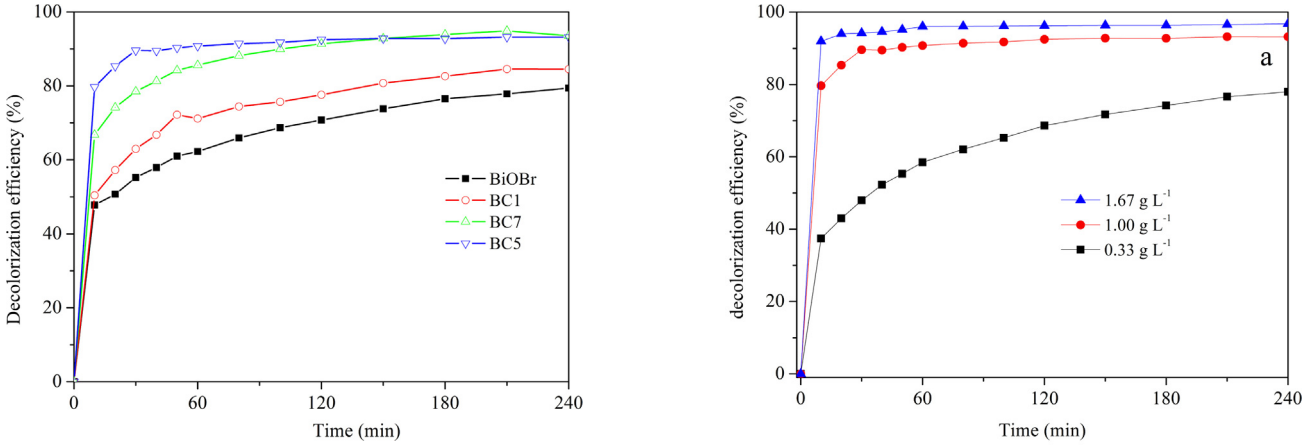

Fig. 8. Comparison of photocatalytic activities of BiOBr, and $BiOBr/CoFe_2O_4$ microspheres on the decolorization of CR solution under simulated solar light irradiation.

Fig. 9. Effects of catalyst dosage (a) and initial concentration (b) on decolorization efficiency of CR solution under simulated solar light irradiation.

as high as that of the pure BiOBr ($0.0650\ min^{-1}$), which results from superior adsorption and transfer performance to organic contaminants in aqueous systems [31]. Considering high efficiency, low price and expectant magnetic performance, $BiOBr/CoFe_2O_4$ weight ratio is controlled in 5:5 for the subsequent photocatalysis decolorization of CR dye by $BiOBr/CoFe_2O_4$ microspheres.

3.3. *Effect of initial CR concentration and photocatalyst dosage*

It is important to study the dependence of photocatalytic decolorization efficiency on initial pollutant concentration and photocatalyst dosage from an application standpoint of view [56]. Different amounts of $BiOBr/CoFe_2O_4$ microspheres ranging from $0.33\ g\ L^{-1}$ to $1.67\ g\ L^{-1}$ for $15\ mg\ L^{-1}$ CR solutions were employed in this study and the corresponding result is shown in Fig. 9a. An obvious increase of decolorization efficiency of CR solution is observed with the increase of photocatalyst amount from $0.33\ g\ L^{-1}$ to $1.0\ g\ L^{-1}$. However, further increase of catalyst amount over $1.0\ g\ L^{-1}$ causes fewer enhancements on decolorization efficiency of CR by $BiOBr/CoFe_2O_4$ microspheres. The reaction rate constants were calculated from the linear fits of each logarithmic plot of decolorization efficiency as a function of irradiation time. As photocatalyst dosage increased from $0.33\ g\ L^{-1}$ to $1.0\ g\ L^{-1}$ the decolorization kinetic rate constant increased obviously, and reached $0.0135\ min^{-1}$ when photocatalyst dosage was $1.0\ g\ L^{-1}$. The increase of photocatalyst dosage increased the number of active sites, consequently both absorbed dye molecules and photons increased [3]. However, at higher photocatalyst dosage beyond $1.0\ g\ L^{-1}$, the rate constant increase is not obvious due to the hindrance and blocking of simulated solar light penetration caused by the excessive amount of photocatalyst. From the viewpoint of practical application, the optimum dosage of $BiOBr/CoFe_2O_4$ microspheres ($1.0\ g\ L^{-1}$) for a given concentration of $15\ mg\ L^{-1}$ of CR solution is moderate. Effects of the initial CR concentration on the decolorization efficiency by the $BiOBr/CoFe_2O_4$

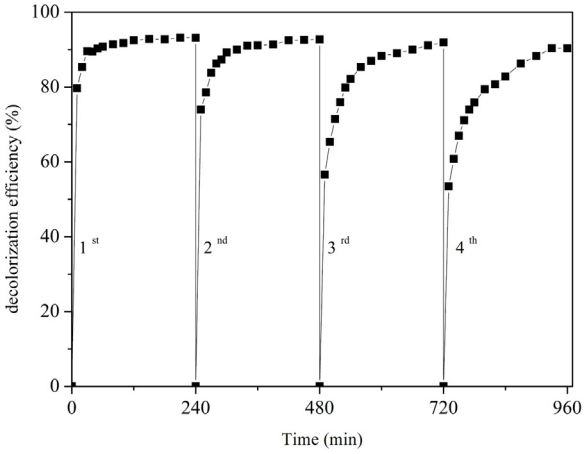

Fig. 10. Cycling runs in the photocatalytic degradation of CR in the presence of $BiOBr/CoFe_2O_4$ microspheres under simulated solar light irradiation.

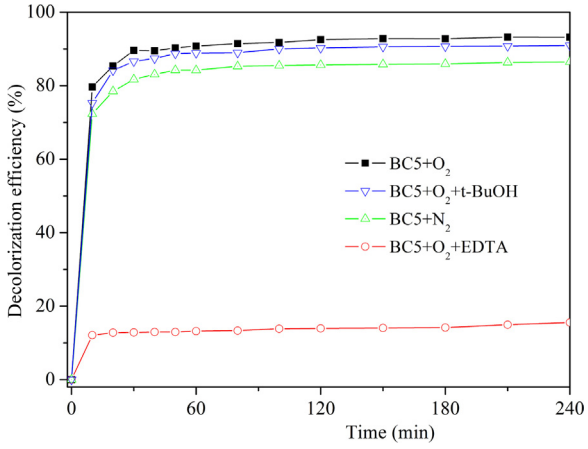

Fig. 11. Photocatalytic decolorization of CR over the $BiOBr/CoFe_2O_4$ microspheres in the present of different scavengers under simulated light irradiation.

microspheres were investigated. Fig. 9b shows the effect of initial CR concentration on photocatalytic decolorization in the presence of 1.0 g L^{-1} $BiOBr/CoFe_2O_4$ microspheres at natural pH. With the increase of initial dye concentration, the decolorization efficiency decreased. The possible explanation is that as the initial concentration of CR increases, the path length of the photons entering the solution decreases. At lower concentration the reversal effect occurred, thereby increasing the number of photon absorbed by $BiOBr/CoFe_2O_4$ microspheres.

3.4. Photocatalytic stability of the photocatalysts

In consideration of practical applications, the photocatalyst should be chemically and optically stable after several repeated trials [57]. The circulating runs in the photocatalytic degradation of CR in the presence of $BiOBr/CoFe_2O_4$ microspheres under simulated solar light were taken to evaluate the stability. Fig. 10 showed the results of CR degradations for four runs. $BiOBr/CoFe_2O_4$ microspheres exhibit remarkable photostability as the CR decolorization efficiency are 93.20%, 92.73%, 91.92%, and 90.36% in the first, second, third, and forth run, respectively. The decrease in the activity of the photocatalyst is only 2.84% after four runs; hence, $BiOBr/CoFe_2O_4$ microspheres can be recycled and reused, which means the photocatalytic decolorization process can be operated in a relatively low cost.

3.5. Role of active species and photocatalytic mechanism

The active species such as trapped holes (h^+), superoxide radical ($O_2^{\bullet-}$) and hydroxyl radical ($^\bullet$OH) are always considered to be the main reasons for the photodegradation of organic pollutant [4,13,58]. For detecting the main active species during photocatalytic reaction, hydroxyl radical ($^\bullet$OH), hole (h^+), and $O_2^{\bullet-}$ were investigated by adding t-BuOH (a quencher of radical scavenger), EDTA-2Na (holes scavenger) and N_2 ($O_2^{\bullet-}$ scavenger), respectively [27]. As shown in Fig. 11, the decolorization efficiency of CR solution decreases notably with the addition of EDTA-2Na compared with that either in the presence of t-BuOH or no addition, indicating that holes are the main reactive species for the photocatalytic decolorization efficiency of CR solution by $BiOBr/CoFe_2O_4$ microspheres [26]. According to previous literature, the conduction band (CB) and valence band (VB) potentials of BiOBr are 0.27 and 3.19 eV, respectively. Therefore, the BiOBr-based photocatalytic reaction under visible light irradiation occurs through the direct oxidation of photogenerated hole with the substrates since it is insufficient for the photogenerated valence band hole of BiOBr to oxidize water to $^\bullet$OH

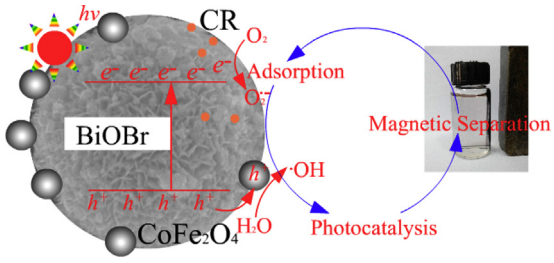

Fig. 12. Schematic diagram of dye decolorization by $BiOBr/CoFe_2O_4$ microspheres under simulated solar light irradiation.

[59]. To test the role of the dissolved oxygen in the degradation process, enough nitrogen (N_2) was bubbled into the suspension to ensure that the reaction system was operated under anoxic conditions. In the presence of N_2, photocatalytic decolorization of CR solution was inhibited compared with that in the presence of O_2 under the same conditions. The result indicated that $O_2^{\bullet-}$ radicals play a role in the photocatalytic decolorization of CR solution by $BiOBr/CoFe_2O_4$ microspheres since $O_2^{\bullet-}$ radicals can be formatted via direct reduction of dissolved oxygen [27]. In a word, the h^+ radicals and $O_2^{\bullet-}$ radicals are considered the two main active species that drive the photodegradation of organic pollutant by $BiOBr/CoFe_2O_4$ microspheres under simulated solar light irradiation.

Based on the above discussion, the possible mechanism of decolorization of CR solution by $BiOBr/CoFe_2O_4$ microspheres has been established and discussed. As shown in Fig. 12, CR molecules were firstly adsorbed fast by $BiOBr/CoFe_2O_4$ microspheres (Eq. (2)) [14,39,60], which led to occur a dye-sensitized reaction of semiconductor [61]. At the same time, the dye-sensitized BiOBr semiconductors in $BiOBr/CoFe_2O_4$ microspheres were excited by simulated solar light irradiation, which induced the generation of electron–hole (e^-/h^+) pairs (Eq. (3)) [11]. The presence of $CoFe_2O_4$ of $BiOBr/CoFe_2O_4$ microspheres led to a more efficient charge separation from BiOBr semiconductor since the introduction of $CoFe_2O_4$ can enhance the photoluminescent intensity of metal oxides (Eq. (4)) [62,63]. Following, the migrated e^- reacted with the oxygen molecule (O_2) that dissolved in aqueous solution to generate $O_2^{\bullet-}$ (Eq. (5)) [64]. The part h^+ radicals reacted with H_2O molecules in solution to generate reactive hydroxyl ($^\bullet$OH) and H^+ ions (Eq. (6)) [12]. Then the photoinduced holes (h^+) directly oxidized the CR dye pollutants to generate the activated CR^+, which then reacted with generated $O_2^{\bullet-}$ radicals or $^\bullet$OH radicals to generate H_2O, CO_2 and other small ultimate byproducts (Eqs. (8) and (9)).

Generally speaking, Eqs. (2), (3), (7) and (8) are the main reaction since the h^+ and $O_2^{\bullet-}$ radicals are the two main active species according to the radical trapping experiments. After magnetic separation, $BiOBr/CoFe_2O_4$ microspheres can be reused to treat other fresh CR solutions.

$$CR(inaqueoussolution) + BiOBr/CoFe_2O_4 \rightarrow CR - BiOBr/CoFe_2O_4 \quad (2)$$

$$BiOBr + h\nu \rightarrow BiOBr(e_{CB}^-) + BiOBr(h_{VB}^+) \quad (3)$$

$$BiOBr(h_{VB}^+) + CoFe_2O_4 \rightarrow BiOBr + CoFe_2O_4(h_{VB}^+) \quad (4)$$

$$BiOBr(e_{CB}^-) + O_2 \rightarrow O_2^{\bullet-} + BiOBr \quad (5)$$

$$CoFe_2O_4(h_{VB}^+) + H_2O \rightarrow {}^{\bullet}OH + H^+ + CoFe_2O_4 \quad (6)$$

$$CR + CoFe_2O_4(h_{VB}^+) \rightarrow CR^+ + CoFe_2O_4 \quad (7)$$

$$CR^+ + O_2^{\bullet-} \rightarrow CO_2 + H_2O + otherbyproducts \quad (8)$$

$$CR^+ + {}^{\bullet}OH \rightarrow CO_2 + H_2O + otherbyproducts \quad (9)$$

4. Conclusions

In summary, novel magnetically separable $BiOBr/CoFe_2O_4$ microspheres were successfully prepared by a facile solvothermal method. The photocatalytic experiments showed that $BiOBr/CoFe_2O_4$ microspheres are a highly active photocatalyst for the decolorization of Congo red under simulated solar light irradiation. Furthermore, the magnetic property of the $BiOBr/CoFe_2O_4$ microspheres facilitate their easy and fast separation from the aqueous solution using an external magnetic field, and the $BiOBr/CoFe_2O_4$ microspheres could be reused for 4 cycles without obvious loss of its reactivity under simulated solar light irradiation.

Acknowledgments

This research was supported by the Natural Science Foundation of Zhejiang Province (Grant Nos. LY14B070011 and LY15E080002) and the National Natural Science Foundation of China (Grant No. 51208331), the China Scholarship Council (Grant No. 201308330411) and Special Funds of Innovative Research Team on Plant Evolutionary Ecology.

References

[1] E. Brillas, C.A. Martínez-Huitle, Decontamination of wastewaters containing synthetic organic dyes by electrochemical methods, an updated review, Appl. Catal. B 166–167 (2015) 603–643.
[2] Y.R. Jiang, H.P. Lin, W.H. Chung, Y.M. Dai, W.Y. Lin, C.C. Chen, Controlled hydrothermal synthesis of BiO_xCl_y/BiOmIn composites exhibiting visible-light photocatalytic degradation of crystal violet, J. Hazard. Mater. 283 (2015) 787–805.
[3] H.Y. Zhu, R. Jiang, L. Xiao, Y.H. Chang, Y.J. Guan, X.D. Li, G.M. Zeng, Photocatalytic decolorization and degradation of Congo red on innovative crosslinked chitosan/nano-CdS composite catalyst under visible light irradiation, J. Hazard. Mater. 169 (2009) 933–940.
[4] W. Cui, W. An, L. Liu, J. Hu, Y. Liang, Synthesis of CdS/BiOBr composite and its enhanced photocatalytic degradation for rhodamine B, Appl. Surf. Sci. 319 (2014) 298–305.
[5] W. An, W. Cui, Y. Liang, J. Hu, L. Liu, Surface decoration of $BiPO_4$ with BiOBr nanoflakes to build heterostructure photocatalysts with enhanced photocatalytic activity, Appl. Surf. Sci. 351 (2015) 1131–1139.
[6] P. Madhusudan, J. Zhang, B. Cheng, G. Liu, Photocatalytic degradation of organic dyes with hierarchical $Bi_2O_2CO_3$ microstructures under visible light, CrystEngComm 15 (2013) 231–240.
[7] H.Y. Zhu, R. Jiang, Y.Q. Fu, Y.J. Guan, J. Yao, L. Xiaog, G.M. Zeng, Effective photocatalytic decolorization of methyl orange utilizing TiO_2/ZnO/chitosan nanocomposite films under simulated solar irradiation, Desalination 286 (2012) 41–48.
[8] L. Ding, R. Wei, H. Chen, J. Hu, J. Li, Controllable synthesis of highly active BiOCl hierarchical microsphere self-assembled by nanosheets with tunable thickness, Appl. Catal. B 172–173 (2015) 91–99.
[9] R. He, S. Cao, P. Zhou, J. Yu, Recent advances in visible light Bi-based photocatalysts, Chin. J. Catal. 35 (2014) 989–1007.
[10] J. Li, Y. Yu, L. Zhang, Bismuth oxyhalide nanomaterials: layered structures meet photocatalysis, Nanoscale 6 (2014) 8473–8488.
[11] L. Lin, M. Huang, L. Long, D. Chen, Novel photocatalysts of fly ash cenospheres supported BiOBr hierarchical microspheres with high photocatalytic performance, J. Alloys Compd. 615 (2014) 929–932.
[12] S.L. Wang, L.L. Wang, W.H. Ma, D.M. Johnson, Y.F. Fang, M.K. Jia, Y.P. Huang, Moderate valence band of bismuth oxyhalides (BiOXs, X = Cl, Br, I) for the best photocatalytic degradation efficiency of MC–LR, Chem. Eng. J. 259 (2015) 410–416.
[13] M. He, W. Li, J. Xia, L. Xu, J. Di, H. Xu, S. Yin, H. Li, M. Li, The enhanced visible light photocatalytic activity of yttrium-doped BiOBr synthesized via a reactable ionic liquid, Appl. Surf. Sci. 331 (2015) 170–178.
[14] Y. Huo, R. Hou, X. Chen, H. Yin, Y. Gao, H. Li, BiOBr visible-light photocatalytic film in rotating disk reactor for organics degradation, J. Mater. Chem. A (2015), http://dx.doi.org/10.1039/c0xx00000x.
[15] O. Mehraj, N.A. Mir, B.M. Pirzada, S. Sabir, Fabrication of novel Ag_3PO_4/BiOBr heterojunction with high stability and enhanced visible-light-driven photocatalytic activity, Appl. Surf. Sci. 332 (2015) (2015) 419–429.
[16] C. Xue, J. Xia, T. Wang, S. Zhao, G. Yang, B. Yang, Y. Dai, G. Yang, A facile and efficient solvothermal fabrication of three-dimensionally hierarchical BiOBr microspheres with exceptional photocatalytic activity, Mater. Lett. 133 (2014) 274–277.
[17] X.C. Song, W.T. Li, W.Z. Huang, H. Zhou, Y.F. Zheng, H.Y. Yin, A novel pen heterojunction BiOBr/$ZnWO_4$: preparation and its improved visible light photocatalytic activity, Mater. Chem. Phys. 160 (2015) 251–256.
[18] X. Meng, Z. Zhang, Synthesis, analysis, and testing of BiOBr–Bi_2WO_6 photocatalytic heterojunction semiconductors, Int. J. Photoenergy (2015), http://dx.doi.org/10.1155/2015/630476.
[19] Z.S. Liu, B.T. Wu, J.N. Niu, P.Z. Feng, Y.B. Zhu, $BiPO_4$/BiOBr p–n junction photocatalysts: one-pot synthesis and dramatic visible light photocatalytic activity, Mater. Res. Bull. 63 (2015) 187–193.
[20] Z. Yang, J. Li, F. Cheng, Z. Chen, X. Dong, BiOBr/protonated graphitic C_3N_4 heterojunctions: intimate interfaces by electrostatic interaction and enhanced photocatalytic activity, J. Alloys Compd. 634 (2015) 215–222.
[21] Y. Gao, H. Huang, Y. He, N. Tian, T. Zhang, P.K. Chu, Q. An, Y. Zhang, In situ crystallization for fabrication of core-satellites structured BiOBr–CdS heterostructure with an excellent visible-light-responsive photoreactivity, Nanoscale 7 (2015) 11702–11711.
[22] W. Cui, W. An, L. Liu, J. Hu, Y. Liang, Novel PbS quantum dots sensitized flower-like BiOBr with enhanced photocatalytic properties under visible light, Mater. Lett. 132 (2014) 251–254.
[23] H.Y. Zhu, R. Jiang, S.H. Huang, J. Yao, F.Q. Fu, J.B. Li, Novel magnetic $NiFe_2O_4$/multi-walled carbon nanotubes hybrids: facile synthesis, characterization, and application to the treatment of dyeing wastewater, Ceram. Int. 41 (2015) 11625–11631.
[24] C. Guo, Y. He, P. Du, X. Zhao, J. Lv, W. Meng, Y. Zhang, J. Xu, Novel magnetically recoverable BiOBr/iron oxides heterojunction with enhanced visible light-driven photocatalytic activity, Appl. Surf. Sci. 320 (2014) 383–390.
[25] Y. Wang, J. Ning, E. Hu, C. Zheng, Y. Zhong, Y. Hu, Direct coating ZnO nanocrystals onto 1D Fe_3O_4/C composite microrods as highly efficient and reusable photocatalysts for water treatment, J. Alloys Compd. 637 (2015) 301–307.
[26] Y. Xu, T. Zhou, S. Huang, M. Xie, H. Li, H. Xu, J. Xia, H. Li, Preparation of magnetic Ag/AgCl/$CoFe_2O_4$ composites with high photocatalytic and antibacterial ability, RSC Adv. 5 (2015) 41475–41483.
[27] Y. Yao, J. Qin, H. Chen, F. Wei, X. Liu, J. Wang, S. Wang, One-pot approach for synthesis of N-doped TiO_2/$ZnFe_2O_4$ hybrid as an efficient photocatalyst for degradation of aqueous organic pollutants, J. Hazard. Mater. 291 (2015) 28–37.
[28] H.L. Andersen, M. Christensen, In situ powder X-ray diffraction study of magnetic $CoFe_2O_4$ nanocrystallite synthesis, Nanoscale 7 (2015) 3481–3490.
[29] C. Cannas, A. Ardu, A. Musinu, L. Suber, G. Ciasca, H. Amenitsch, G. Campi, Hierarchical formation mechanism of $CoFe_2O_4$ mesoporous assemblies, ACS Nano 9 (2015) 7277–7286.
[30] L. Deng, Z. Shi, X. Peng, Adsorption of Cr(VI) onto a magnetic $CoFe_2O_4$/MgAl-LDH composite and mechanism study, RSC Adv. 5 (2015) 49791–49801.
[31] Y. Fu, H. Chen, X. Sun, X. Wang, Combination of cobalt ferrite and graphene: high-performance and recyclable visible-light photocatalysis, Appl. Catal. B 111–112 (2012) 280–287.
[32] K. Gandha, K. Elkins, N. Poudyal, J.P. Liu, Synthesis and characterization of $CoFe_2O_4$ nanoparticles with high coercivity, J. Appl. Phys. (2015), http://dx.doi.org/10.1063/1.4916544.
[33] H. Hamad, M.A. El-Latif, A.E. Kashyout, W. Sadik, M. Feteha, Synthesis and characterization of core–shell–shell magnetic ($CoFe_2O_4$–SiO_2–TiO_2) nanocomposites and TiO_2 nanoparticles for the evaluation of photocatalytic activity under UV and visible irradiation, New J. Chem. 39 (2015) 3116–3128.
[34] Z. Lu, M. He, L. Yang, Z. Ma, L. Yang, D. Wang, Y. Yan, W. Shi, Y. Liu, Z. Hua, Selective photodegradation of 2-mercaptobenzothiazole by a novel imprinted $CoFe_2O_4$/MWCNTs photocatalyst, RSC Adv. 5 (2015) 47820–47829.
[35] O.A. Oyetade, V.O. Nyamori, B.S. Martincigh, S.B. Jonnalagadda, Effectiveness of carbon nanotube-cobalt ferrite nanocomposites for the adsorption of rhodamine B from aqueous solutions, RSC Adv. 5 (2015) 22724–22739.

[36] F. Sadri, A. Ramazani, A. Massoudi, M. Khoobi, V. Azizkhani, R. Tarasi, L. Dolatyari, B.K. Min, Magnetic $CoFe_2O_4$ nanoparticles as an efficient catalyst for the oxidation of alcohols to carbonyl compounds in the presence of oxone as an oxidant, Bull. Korean Chem. Soc. 35 (2014) 2029–2032.
[37] Q. Song, Z.J. Zhang, Shape control and associated magnetic properties of spinel cobalt ferrite nanocrystals, J. Am. Chem. Soc. 126 (2004) 6164–6168.
[38] R.S. Yadav, J. Havlica, J. Masilko, L. Kalina, M. Hajdúchová, V. Enev, J. Wasserbauer, I. Kuritka, Z. Kozakova, Structural, cation distribution, and magnetic properties of $CoFe_2O_4$ spinel ferrite nanoparticles synthesized using a starch-assisted sol–gel auto-combustion method, J. Supercond. Nov. Magn. 28 (2015) 1851–1861.
[39] M.A. Khan, M.M. Alam, M. Naushad, Z.A. Alothman, M. Kumar, T. Ahamad, Sol-gel assisted synthesis of porous nano-crystalline $CoFe_2O_4$ composite and its application in the removal of brilliant blue-R from aqueous phase: an eco-friendly and economical approach, Chem. Eng. J. 279 (2015) 416–424.
[40] Y. Ren, L. Lin, J. Ma, J. Yang, J. Feng, Z. Fan, Sulfate radicals induced from peroxymonosulfate by magnetic ferrospinel MFe_2O_4 (M = Co, Cu, Mn, and Zn) as heterogeneous catalysts in the water, Appl. Catal. B 165 (2015) 572–578.
[41] E. Karaoglu, A. Baykal, $CoFe_2O_4$–Pd (0) nanocomposite: magnetically recyclable catalyst, J. Supercond. Nov. Magn. 27 (2014) 2041–2047.
[42] S. Ma, S. Zhan, Y. Jia, Q. Zhou, Highly efficient antibacterial and Pb(II) removal effects of Ag-$CoFe_2O_4$-GO nanocomposite, ACS Appl. Mater. Interfaces 7 (2015) 10576–10586.
[43] Y. Ren, N. li, J. Feng, T. Luan, Q. Wen, Z. Li, M. Zhang, Adsorption of Pb(II) and Cu(II) from aqueous solutions on magnetic porous, J. Colloid Interface Sci. 376 (2012) 415–442.
[44] J. Fu, C.J. DeSantis, R.G. Weiner, S.E. Skrabalak, Aerosol-assisted synthesis of shape-controlled $CoFe_2O_4$: topotactic versus direct melt crystallization, Chem. Mater. 27 (2015) 1863–1868.
[45] Y. Jia, Y. Yang, Y. Guo, W. Guo, Q. Qin, X. Yang, Y. Guo, Simulated sunlight photocatalytic degradation of aqueous p-nitrophenol and bisphenol A in a Pt/BiOBr film-coated quartz fiber photoreactor, Dalton Trans. 44 (2015) 9439–9449.
[46] J. Jiang, X. Zhang, P. Sun, L. Zhang, ZnO/BiOI heterostructures: photoinduced charge-transfer property and enhanced visible-light photocatalytic activity, J. Phys. Chem. C 115 (2011) 20555–20564.
[47] F. Zhao, Y. Zou, X. Lv, H. Liang, Q. Jia, W. Ning, Synthesis of $CoFe_2O_4$–zeolite materials and application to the adsorption of gallium and indium, J. Chem. Eng. Data 60 (2015) 1338–1344.
[48] X. Li, J. Feng, Y. Du, J. Bai, H. Fan, H. Zhang, Y. Peng, F. Li, One-pot synthesis of $CoFe_2O_4$/graphene oxide hybrids and their conversion into FeCo/grapheme hybrids for lightweight and highly efficient microwave absorber, J. Mater. Chem. A 3 (2015) 5535–5546.
[49] Y. Ao, D. Wang, P. Wang, C. Wang, J. Hou, J. Qian, BiOBr/Co-Ni layered double hydroxide nanocomposites with excellent adsorption and photocatalytic properties, RSC Adv. 5 (2015) 54613–54621.
[50] R. Jiang, H.Y. Zhu, H.H. Chen, J. Yao, Y.Q. Fu, Z.Y. Zhang, Y.M. Xu, Effect of calcination temperature on physical parameters and photocatalytic activity of mesoporous titania spheres using chitosan/poly (vinyl alcohol) hydrogel beads as a template, Appl. Surf. Sci. 319 (2014) 189–196.
[51] Z.-C. Zhu, P. Chen, X.-H. Yang, R.-X. Wang, BiOBr three-dimensional micromaterials in a solvothermal system and their photocatalytical property under visible-light irradiation, J. Exp. Nanosci. 10 (2015) 564–575.
[52] D. Moitra, S. Hazra, B.K. Ghosh, R.K. Jani, M.K. Patra, S.R. Vadera, N.N. Ghosh, A facile low temperature method for the synthesis of $CoFe_2O_4$ nanoparticles possessing excellent microwave absorption properties, RSC Adv. 5 (2015) 51130–51134.
[53] T. Harifi, M. Montazer, A novel magnetic reusable nanocomposite with enhanced photocatalytic activities for dye degradation, Sep. Purif. Technol. 134 (2014) 210–219.
[54] L. Gan, S. Shang, C.W.M. Yuen, S. Jiang, E. Hu, Hydrothermal synthesis of magnetic $CoFe_2O_4$/grapheme nanocomposites with improved photocatalytic activity, Appl. Surf. Sci. 351 (2015) 140–147.
[55] S. Kaur, V. Singh, TiO_2 mediated photocatalytic degradation studies of Reactive Red 198 by UV irradiation, J. Hazard. Mater. 141 (2007) 230–236.
[56] H.Y. Zhu, R. Jiang, Y.G. Guan, Y.Q. Fu, X. Ling, G.M. Zeng, Effect of key operational factors on decolorization of methyl orange during H_2O_2 assisted CdS/TiO_2/ploymer nanocomposite thin films under simulated solar light irradiation, Sep. Purif. Technol. 74 (2010) 187–194.
[57] Q. Yu, A. Fu, H. Li, H. Liu, R. Lv, J. Liu, P. Guo, X.S. Zhao, Synthesis and characterization of magnetically separable Ag nanoparticles decorated mesoporous Fe_3O_4@carbon with antibacterial and catalytic properties, Colloids Surf. A 457 (2014) 288–296.
[58] W. Zhang, B. Jia, Q. Wang, D. Dionysiou, Visible-light sensitization of TiO_2 photocatalysts via wet chemical N-doping for the degradation of dissolved organic compounds in wastewater treatment: a review, J. Nanoparticle Res. 17 (2015) 221–232.
[59] X. Zhang, R. Li, M. Jia, S. Wang, Y. Huang, C. Chen, Degradation of ciprofloxacin in aqueous bismuth oxybromide (BiOBr) suspensions under visible light irradiation: a direct hole oxidation pathway, Chem. Eng. J. 274 (2015) 290–297.
[60] P.N. Medeiros, Y.F. Gomes, M.R.D. Bomio, I.M.G. Santos, M.R.S. Silva, C.A. Paskocimas, M.S. Li, F.V. Motta, Influence of variables on the synthesis of $CoFe_2O_4$ pigment by the complex polymerization method, J. Adv. Ceram. 4 (2015) 135–141.
[61] Y. Lei, G. Wang, P. Guo, H. Song, The Ag-$BiOBr_xI_{1-x}$ composite photocatalyst: preparation, characterization and their novel pollutants removal property, Appl. Surf. Sci. 279 (2013) 374–379.
[62] F. Bi, X. Dong, J. Wang, G. Liu, Coaxial electrospinning preparation and properties of magnetic-photoluminescent bifunctional $CoFe_2O_4$@Y_2O_3: Eu^{3+} coaxial nanofibers, J. Mater. Sci.: Mater. Electron. 25 (2014) 4259–4267.
[63] Y. Jia, Z. Zhou, Y. Wei, Z. Wu, J. Chen, Y. Zhang, Y. Liu, Magnetization-induced enhancement of photoluminescence in core–shell $CoFe_2O_4$@YVO_4: Eu^{3+} composite, J. Appl. Phys. 114 (2013), 213903-213903-4.
[64] W. Li, Y. Tian, P. Li, B. Zhang, H. Zhang, W. Geng, Q. Zhang, Synthesis of rattle-type magnetic mesoporous Fe_3O_4@mSiO_2@BiOBr hierarchical photocatalyst and investigation of its photoactivity in the degradation of methylene blue, RSC Adv. 5 (2015) 48050–48059.

《SCI-Expanded》收录及《JCR》期刊影响因子证明

经检索《Web of Science》和《Journal Citation Reports（JCR）》数据库，《Science Citation Index Expanded (SCI-EXPANDED)》收录论文及其期刊影响因子如下。（检索时间 2016 年 6 月 16 日）

第 1 条，共 1 条

标题: Fabrication of novel magnetically separable BiOBr/CoFe2O4 microspheres and its application in the efficient removal of dye from aqueous phase by an environment-friendly and economical approach

作者: Jiang, R(Jiang, R.);Zhu, HY(Zhu, H. -Y.);Li, JB(Li, J. -B.);Fu, FQ(Fu, F. -Q.);Yao, J(Yao, J.);Jiang, ST(Jiang, S. -T.);Zeng, GM(Zeng, G. -M.);

来源出版物:APPLIED SURFACE SCIENCE

卷:364 **页:**604-612**DOI:**10.1016/j.apsusc.2015.12.200 **出版年:**FEB 28 2016

入藏号:WOS:000369957800077

文献类型: Article

地址:

[Jiang, R.; Zhu, H. -Y.; Fu, F. -Q.; Yao, J.] Taizhou Univ, Zhejiang Prov Key Lab Plant Evolutionary Ecol & C, Taizhou 318000, Zhejiang, Peoples R China.

[Jiang, R.; Zhu, H. -Y.; Li, J. -B.] Univ British Columbia, Environm Engn Program, Prince George, BC V2N 4Z9, Canada.

[Jiang, R.; Zhu, H. -Y.; Yao, J.; Jiang, S. -T.] Taizhou Univ, Dept Environm Engn, Taizhou 318000, Zhejiang, Peoples R China.

[Zeng, G. -M.] Hunan Univ, Minist Educ, Key Lab Environm Biol & Pollut Control, Changsha 410082, Hunan, Peoples R China.

通讯作者地址:

Zeng, GM (reprint author), Hunan Univ, Minist Educ, Key Lab Environm Biol & Pollut Control, Changsha 410082, Hunan, Peoples R China.; Zhu, HY (reprint author), 1139 Municipal Govt Ave, Taizhou City 318000, Zhejiang, Peoples R China.

电子邮件地址:zhuhuayue@126.com; zgming@hnu.cn

IDS 号:DD5IW

ISSN:0169-4332

期刊《APPL SURF SCI》2015 年 JCR 的影响因子为 3.150。

注：

1. 因 JCR 的最新数据截止到 2015 年，2016 年出版期刊的影响因子以 2015 年的影响因子为参考。
2. 以上检索结果来自 CALIS 查收查引系统。
3. 以上检索结果均得到委托人及被检索作者的确认。

教育部科技查新工作站(Z09)

检索人(签章):何晓薇

2016 年 6 月 16 日